Deep-Sea Research I 103 (2015) 125–136

Contents lists available at ScienceDirect

Deep-Sea Research I

journal homepage: www.elsevier.com/locate/dsri

The fate of the Deep Western Boundary Current in the South Atlantic

Silvia L. Garzoli [a,b,*], Shenfu Dong [a,b], Rana Fine [c], Christopher S. Meinen [b], Renellys C. Perez [a,b], Claudia Schmid [b], Erik van Sebille [d,e], Qi Yao [a,b]

[a] Cooperative Institute for Marine and Atmospheric Studies, University of Miami, USA
[b] NOAA/Atlantic Oceanographic and Meteorological Laboratory, USA
[c] Rosenstiel School of Marine and Atmospheric Sciences, University of Miami, USA
[d] ARC Centre of Excellence for Climate System Science & Climate Change Research Centre, UNSW, Sydney, New South Wales, Australia
[e] Grantham Institute & Department of Physics, Imperial College London, London, United Kingdom

ARTICLE INFO

Article history:
Received 29 January 2015
Received in revised form
24 April 2015
Accepted 31 May 2015
Available online 25 June 2015

Keywords:
Meridional Overturning Circulation
North Atlantic Deep Water
Deep Western Boundary Current
South Atlantic Circulation

ABSTRACT

The pathways of recently ventilated North Atlantic Deep Water (NADW) are part of the lower limb of the Atlantic Meridional Overturning Circulation (AMOC). In the South Atlantic these pathways have been the subject of discussion for years, mostly due to the lack of observations. Knowledge of the pathways of the AMOC in the South Atlantic is a first order prerequisite for understanding the fluxes of climatically important properties. In this paper, historical and new observations, including hydrographic and oxygen sections, Argo data, and chlorofluorocarbons (CFCs), are examined together with two different analyzes of the Ocean general circulation model For the Earth Simulator (OFES) to trace the pathway of the recently ventilated NADW through the South Atlantic. CLIVAR-era CFCs, oxygen and salinity clearly show that the strongest NADW pathway in the South Atlantic is along the western boundary (similar to the North Atlantic). In addition to the western boundary pathway, tracers show an eastward spreading of NADW between ~17 and 25°S. Analyzed together with the results of earlier studies, the observations and model output presented here indicate that after crossing the equator, the Deep Western Boundary Current (DWBC) transports water with the characteristics of NADW and a total volume transport of approximately 14 Sv (1 Sv=10^6 m^3 s^{-1}). It crosses 5°S as a narrow western boundary current and becomes dominated by eddies further south. When this very energetic eddying flow reaches the Vitória-Trindade Ridge (~20°S), the flow follows two different pathways. The main portion of the NADW flow continues along the continental shelf of South America in the form of a strong reformed DWBC, while a smaller portion, about 22% of the initial transport, flows towards the interior of the basin.

1. Introduction

The role of the southward flowing Deep Western Boundary Current (DWBC) as a primary pathway for the cold, lower limb of the Atlantic Meridional Overturning Circulation (AMOC) has been well documented in the North Atlantic Ocean (e.g. Molinari et al., 1998; Schott et al., 2004; Johns et al., 2008; Meinen et al., 2012)[1]. However the pathways and variability of the DWBC as the lower limb of the overturning circulation in the South Atlantic Ocean are less well established. Much of what is known about the deep flows in the South Atlantic has been inferred from the merging of hydrographic sections in the region. They are used to trace the North Atlantic Deep Water (NADW), the main water mass carried by the DWBC. For example, Reid's (1989) maps of geopotential anomaly of the 3000 db surface with respect to the 3500 db surface indicate that part of the NADW from the DWBC flows to the interior near 25°S producing eastward tongues of high salinity and oxygen extending close to the Mid-Atlantic Ridge. Reid's analysis of salinity, oxygen, phosphate, and silica also suggests eastward flow towards the interior.

There are few direct observations of the DWBC in the South Atlantic. A two year-long velocity and temperature time series from a moored array, shipboard observations, and model simulations previously suggested that the southward flowing DWBC breaks up into eddies before reaching 8°S (Dengler et al., 2004). They reported that between 8°S and 16°S, the transport of NADW into the South Atlantic Ocean is accomplished by southeastward migrating eddies, rather than by a continuous flow. Direct current

* Corresponding author at: CIMAS, University of Miami and NOAA/Atlantic Oceanographic and Meteorological Laboratory, Miami, USA. Fax: +1 305 361 4392.

[1] Note: One exception to this is near and south of the Grand Banks of Newfoundland, where Lagrangian floats suggest that the DWBC flow breaks up and interacts significantly with the interior (e.g. Bower et al., 2009).

http://dx.doi.org/10.1016/j.dsr.2015.05.008
0967-0637/

meter observations by Schott et al. (2005) supported the idea that a mean DWBC exists at 5°S and dissolves into a sequence of deep eddies between 5°S and 11°S. Hogg and Owens (1999) analyzed observations collected from Lagrangian floats launched as part of the Deep Basin Experiment. They concluded that the line of sea mounts that extends eastward from the South American coast just south of 20°S rising to depths of 2000 m or less at places, (known as the Vitória-Trindade Ridge), interrupts the southward-flowing DWBC and is the location for significant eddy exchange into the interior. Their float trajectories provided little indication of a continuation of the DWBC flowing southward beyond the Vitória-Trindade Ridge, although a single float trajectory did return to the western boundary south of 20°S.

Further south, direct current measurements (Muller et al., 1998) and geostrophic current estimates (Zangenberg and Siedler, 1998) have hinted at the existence of a DWBC along the continental slope between 20°S and 28°S, with a southward transport that ranges between 2 and 10 Sv ($1\ \mathrm{Sv}=10^6\ \mathrm{m^3\ s^{-1}}$). This might suggest the presence of at least a portion of the DWBC along the western boundary south of the Vitória-Trindade Ridge. A more recent study (Meinen et al., 2012) used data from a line of four pressure equipped inverted echo sounders (PIES) as well as hydrographic and dissolved oxygen (O_2) measurements to study the DWBC along 34.5°S on the South American continental shelf/slope. These data have confirmed the presence of a DWBC with water mass characteristics of NADW (elevated oxygen and salinity) at 34.5°S.

On the other side of the Atlantic basin at 30°S, hydrographic sections have also been used to show southward flow of water with characteristics of NADW along the eastern boundary and a mean transport of 3 Sv (Arhan et al., 2003). These observations are consistent with a portion of the NADW perhaps having followed an interior pathway over to the eastern boundary. Because of the paucity of observations to date, the details of this interior pathway are still quite uncertain.

Enhancements to the suite of measurements made during hydrographic cruises over the past decades allow for these hydrographic data to yield more information on ocean pathways than were previously possible. For example, hydrographic sections of salinity and dissolved oxygen from the WOCE Atlas Volume 3, Atlantic Ocean (http://www-pord.ucsd.edu/whp_atlas/atlantic/sections.htm) show clear evidence of water with the NADW characteristics (i.e., low temperature, $T\sim 3$ °C, and high salinity, $S>34.8$ psu, water with high levels of dissolved oxygen, $O_2>240\ \mu\mathrm{mol\ kg^{-1}}$) along the western boundary at 11°S, 19°S, and 30°S (Koltermann et al., 2011). The NADW can also be traced by looking for waters with high concentrations of chlorofluorocarbons (CFCs) (Fine et al., 2002); recently ventilated NADW carries an elevated CFC concentration because it has been more recently in contact with the atmosphere than the older waters at the same depths that were last in contact with the atmosphere before the measurable CFC transient (~1960s). The high CFC NADWs flow equatorward from the high latitude North Atlantic in the DWBC (e.g., Fine and Molinari, 1988) and along the equator (Weiss et al., 1985). Wanninkhof et al. (2010) analyzed repeat observations from the meridional Atlantic section A16 along ~25°W from Iceland to 56°S. The composite quasi-meridional sections from the 2003 and 2005 A16 cruises for salinity, apparent oxygen utilization, total dissolved inorganic carbon, nitrate, and silicate show that water masses with NADW properties are present at 20°S in the center of the basin (~25°W).

Numerical models have also been used to improve our understanding of the spreading of the NADW into the South Atlantic. Speich et al. (2007) computed trajectories of the particles that represent the southward flow of NADW at 44°N in the North Atlantic (i.e., characterized by a potential density anomaly greater than $27.7\ \mathrm{kg\ m^{-3}}$). Trajectories were computed in a coarse-resolution ocean general circulation model (2° uniform zonal resolution, and meridional resolution that varies from 0.5° at the equator to $2°\cos(\phi)$ poleward of the tropics). This coarse resolution Lagrangian simulation shows NADW flowing southward along the coast of South America in the DWBC to approximately 45°S, after which it flows into the interior towards the east. Although analysis of a global eddy-permitting (nominal horizontal resolution of 0.25°) Parallel Ocean Climate Model (POCM) by Matano and Beier (2003) similarly demonstrated the main pathway for the DWBC is along the coast of South America, there were also some indications of another pathway flowing into the interior along approximately 27°S.

More recently, van Sebille et al. (2012) utilized the output from the global high-resolution (0.1° horizontal resolution) Ocean general circulation model For the Earth Simulator (OFES) model to study the NADW pathways in the South Atlantic. They found 3.6 Sv of NADW crossing eastward at about 25°S underneath the trajectory followed by the Agulhas rings that detach from the Agulhas Retroflection and then slowly drift northwestward along the so-called Agulhas ring corridor. They analyzed the velocity and density fields of the last 27-years of output from a 57-year (1950–2006) run of the OFES model and found that the decay of the Agulhas rings, and their forward tilt with depth, results in a southward velocity of 1–2 cm/s across isolines of planetary vorticity in the deep waters. The associated stream function pattern yields a deep circulation transporting about 4 Sv of NADW from the DWBC eastward at 25°S to the southern tip of Africa. The pathway of the DWBC and how it reforms along the western boundary south of 25°S were not the objective of the analysis conducted by van Sebille et al. (2012), and will be analyzed in detail in what follows using the OFES model and available observations.

Previous modeling and observational work has shown that important water mass transformations occur in the South Atlantic (e.g., Garzoli and Matano, 2011, and references therein). For example, transformations occur in the very energetic regions near the boundaries such as the Brazil–Malvinas Confluence and the Cape Basin (Provost et al., 1999; Lumpkin and Speer, 2007; Jullion et al., 2010; Garzoli and Matano, 2011; Rimaud et al., 2012). These water mass transformation regions will both influence and be influenced by the pathways of the DWBC as it flows through the South Atlantic, and the transformations will have important impacts on the AMOC. The stability of the AMOC has been shown to be directly related to meridional salt fluxes between the South Atlantic and other ocean basins (e.g., Drijfhout et al., 2011; Bryden et al., 2011; Garzoli et al., 2013). Developing a detailed knowledge and understanding of the pathways of the lower limb of the AMOC will therefore be crucial for quantifying the fluxes of heat, fresh water, and CO_2 through the South Atlantic and for assessing the stability of the AMOC.

The objective of this paper is to utilize existing and recent hydrographic and tracer data sets, a new gridded subsurface Argo data product (Schmid, 2014), and Eulerian and Lagrangian analyzes from the high-resolution OFES model, to extend the previous work conducted by van Sebille et al. (2012) and to learn more about the western boundary and interior pathways of the NADW in the South Atlantic. Furthermore the transports associated with these pathways will be quantified and will demonstrate the strength of the flow along the western boundary pathway, which has historically been underestimated.

2. Observational evidence

2.1. Pathways based on hydrographic and CFC tracers

The recently ventilated NADW carried by the lower limb of the AMOC is characterized by low temperature (~3 °C), high salinity ($S > 34.8$ psu), and high levels of dissolved oxygen ($O_2 > 240$ μmol kg^{-1}). This NADW flows southward at neutral density levels between 27.9 and 28.1 kg m^{-3} in the South Atlantic near 35°S (Schmitz and McCartney, 1992; Meinen et al., 2012; Preu et al., 2013). Inspection of the CTD sections collected during the WOCE experiment at 11°S, 19°S and 30°S (Koltermann et al., 2011) show that water masses with these characteristics in the South Atlantic are concentrated in the western basin between 1500 and 3000 m depth. At 11°S these water are observed west of 20°W, and at 19°S and 30°S the recently ventilated NADW is found as far offshore as 5°W.

As mentioned in the introduction recently ventilated NADW can be tracked using other CFCs. Using the WOCE data era (1992–1997), maps of chlorofluorocarbon-11 (CFC-11) concentrations are generated via the data-interpolating variational analysis (DIVA) gridding technique (Troupin et al., 2012) applied to the South Atlantic (Fig. 1) on neutral density level 27.9 kg m^{-3}, the level of the upper NADW between 1700 and 2000 m. High concentrations (> 0.03 pmol kg^{-1}) of CFC-11 are observed along the western boundary in the North Atlantic, along the equator, and extending into the South Atlantic along the western boundary north of 5°N (Fig. 1). On the WOCE era map, concentrations above 0.05 pmol kg^{-1} are found extending into the South Atlantic along the western boundary only to ~15°S. However, there is evidence of elevated concentrations (> 0.04 pmol kg^{-1}) of recently ventilated NADW in the interior near 23°S, 35°W. Ventilated NADW is defined here as those waters of NADW origin that carry above blank level CFC-11 (i.e. CFC-11 values > 0.005 pmol kg^{-1}). CFCs are a transient tracer, and they increased in NADW well after the mid-1990 s (e.g., Kieke et al., 2007). As a consequence, the southward and eastward spreading of ventilated NADW is probably limited in the WOCE era data, as they had not yet had time to spread.

To investigate this point further, CLIVAR transect data (repeats of WOCE-era transects obtained during the first two decades of the 2000s) have been analyzed in this study. CFC data in the South Atlantic south of 10°S and north of 40°S were collected along the following CLIVAR sections: A13 ~5–10°E in 2010, A15 20°W in 2000, A16S ~25°W in 2005 and 2013–2014, and A10 ~30°S in 2003 and 2011 (see brown lines in Fig. 1). Although other sections were occupied in the South Atlantic, they did not collect CFC measurements. Thus, there are not enough CLIVAR data with which to make a map of CFC concentrations, similar to what was done for WOCE data of the 1990s (Fig. 1). Instead, data from A10 (~30°S), A16S (~25°W) and A13 (~5–10°E) are presented as individual cross-sections of high CFCs, oxygen and salinity, which are used to show for the first time the eastward spreading of NADW into the central South Atlantic Ocean (Fig. 2).

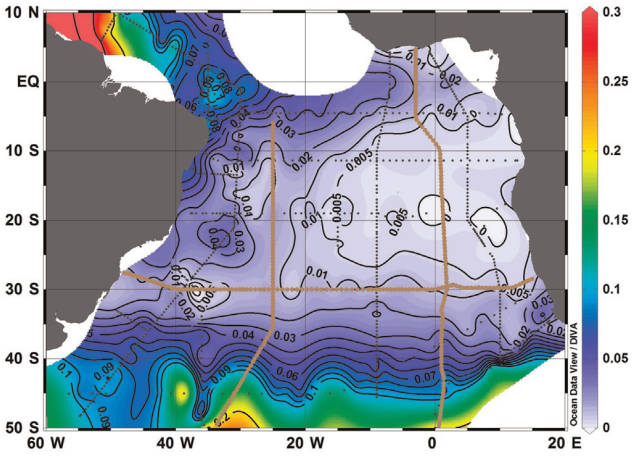

Fig. 1. Map of CFC-11 in pmol kg^{-1} on neutral density level 27.9 kg m^{-3}, the level of the upper NADW, generated from WOCE-era data from 1992 to 1997. Brown lines indicate highlighted WOCE lines: A10 zonal line along 30°S, A16S meridional line at 25°W and A13 meridional line at 0°E. The black dots indicate locations of all of the other WOCE stations used to make this map.

Between ~17 and 25°S the NADW has reached as far east as 25°W during the 2005 (not shown) and 2013–2014 (Fig. 2a–c) occupations and there is a suggestion of elevated CFCs at 5–10°E south of 28°S during the 2010 occupation (Fig. 2d). This can be more clearly seen along 30°S (Fig. 2e), as a large area with elevated CFCs > 0.01 pmol kg^{-1} is observed to extend east of Walvis Ridge between 5 and 15°E. Note that the high tracer cores (CFC-11, salinity and oxygen) are not completely overlapping in space. If the high CFC-11 core in Fig. 2a is taken as 0.04 pmol kg^{-1}, then indeed it does occupy the same depths as the oxygen and salt cores of Fig. 2b and c. Furthermore, the high salinity core reaches upward to almost 1500 m as does the CFC-11, but not oxygen. In addition, highest concentrations of CFC-11 are observed at shallower depths 1500–2400 m in Fig. 2a, as compared with Fig. 2e where the highest CFC-11 is observed at 2000–2400 m. The upper part of the high CFC-11 core in Fig. 2a at approximately 22°S, 25°W is of Labrador Sea origin. A probable explanation for the difference in signatures at the two latitudes is that at 30°S near the western boundary the shallower Labrador Sea Water has been largely replaced with waters of southern origin and lower CFC-11, for example, Upper Circumpolar Deep Water.

Fig. 2e shows the highest subsurface CFC concentrations (> 0.2 pmol kg^{-1}) in NADW along the western boundary at 30°S. High CFCs spreading southward in the WBC is consistent with recent dissolved oxygen measurements collected during hydrographic cruises along the western boundary near 35°S (Schmitz and McCartney, 1992; Meinen et al., 2012; Preu et al., 2013). In time, as the CFC transient penetrates the South Atlantic, on future occupations of the ~25°W, ~5–10°E, and 30°S sections, it may be possible to observe interior eastward flowing NADW that has turned southward near the eastern boundary east of Walvis Ridge. To summarize, the CLIVAR-era CFCs, oxygen and salinity demonstrate that the strongest NADW signal in the South Atlantic (similar to the North Atlantic) is along the western boundary and that there is eastward spreading of NADW between ~17 and 25°S, and NADW is observed east of the Walvis Ridge at 30°S.

2.2. Argo data

The Argo array is a global set of more than 3000 free-drifting floats that sample the upper ocean to a maximum pressure level of 2000 dbar, which is within the upper layer of the NADW. Schmid (2014) developed a procedure to obtain three-dimensional fields of absolute geostrophic velocities from Argo and altimeter data. Results were published for the period ending in June 2012. In an expansion of Schmid (2014), 66,264 profiles of temperature and salinity collected in the South Atlantic in the years 2000–2013, were used to generate an updated product for this study. The 3-D velocity field extends from the surface to 2000 dbar with a vertical resolution of 10 dbar. Velocity fields are derived by first combining *in situ* dynamic height profiles from floats with the sea surface height from AVISO (CLS, 1996) to generate synthetic dynamic height profiles with better spatial and temporal coverage than could be achieved using only the *in situ* observations. This process yields 162 monthly mean dynamic heights covering the period

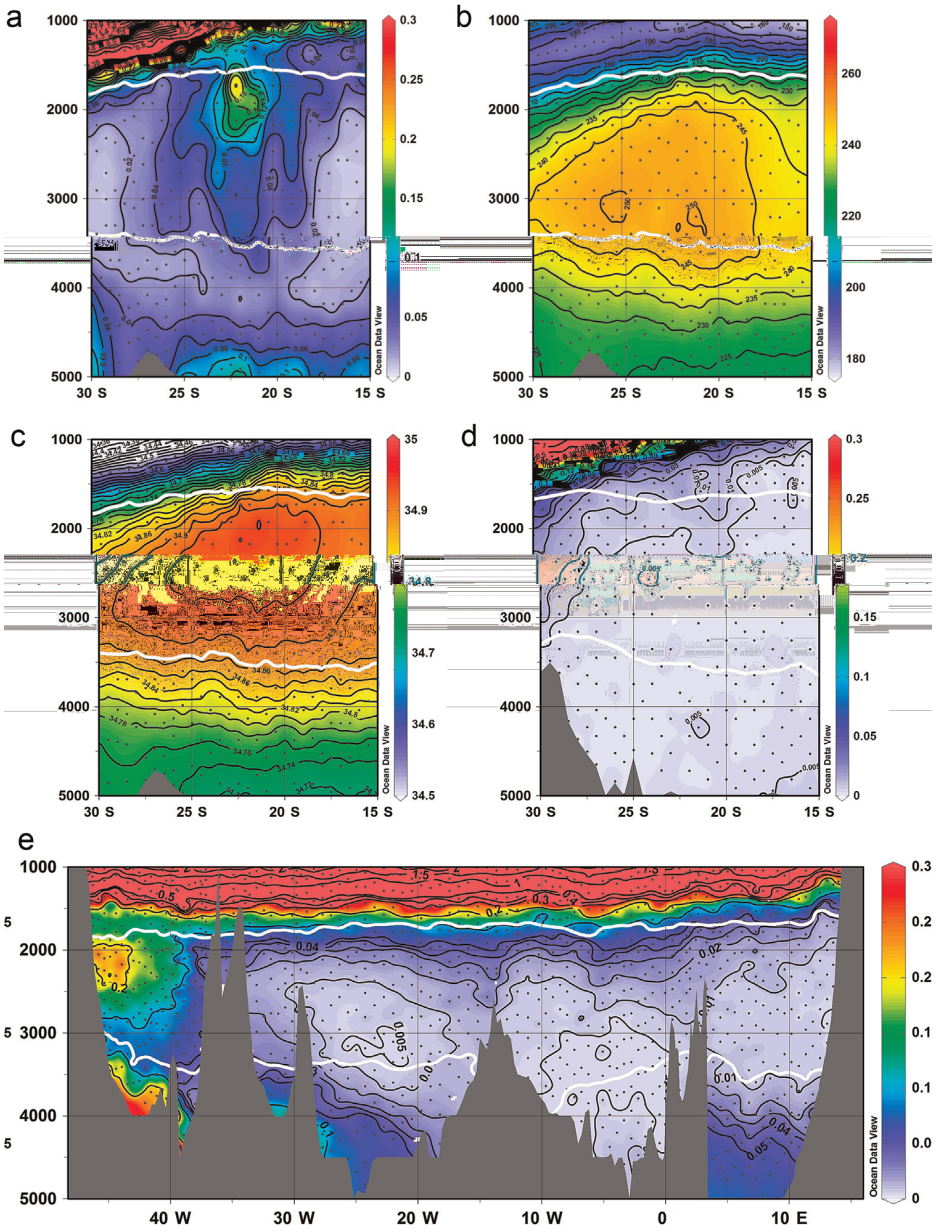

Fig. 2. Partial CLIVAR sections demonstrating the spread of NADW eastward into the central South Atlantic Ocean. Vertical axis is depth in meters. Panel (a) partial A16S section of CFC-11 from 15 to 30°S along about 25°W from 1000 to 5000 m. The lowest contour for CFC-11 concentration is 0.01 pmol kg^{-1}. Color scale given on the right; two neutral density surfaces are 27.9 and 28.1 kg m^{-3} are identified as white lines. Panel (b) Same as panel (a) except for oxygen concentration in μmol kg^{-1}. Panel (c) Same as panel a) except for salinity. Panel (d) Partial A13 section of CFC-11 from 15 to 30°S along about 5–10°E from 1000 to 5000 m. The lowest contour for CFC-11 concentration is 0.005 pmol/kg. Panel (e) full cross-basin section of CFC-11 along A10, 30°S from 1000 to 5000 m. Note for a, d, and e that 0.3 pmol kg^{-1} is the highest concentration CFC-11 contoured and higher concentrations will appear in the same shades as for 0.3 pmol kg^{-1}.

March 2000–August 2013. Dynamic heights are used to calculate geostrophic velocities relative to the reference level of 1000 dbar on a 0.5° longitude by 0.5° latitude grid from 5°S to 50°S. Absolute geostrophic velocity is then estimated using drift velocities obtained from the trajectories of 825 Argo and WOCE floats, which were active from December 9, 1992 to February 20, 2014 and drifted in the pressure range of 800–1100 dbar. These drift velocities, and the associated pressures, are used to derive gridded fields of the absolute velocity (Schmid, 2014). The gridded monthly mean profiles of geostrophic relative velocity are then referenced to the monthly mean float-derived absolute velocities, when available. If no monthly mean absolute velocity estimate is available at a given grid point, then the climatological absolute velocity is used. The resulting monthly mean absolute geostrophic velocity fields are then averaged to generate a 3-D field of the long-term mean of the horizontal velocity.

The long-term mean gridded Argo-derived absolute velocity field at 2000 dbar (within the upper layer of the NADW) is shown in Fig. 3 (top panel). This high-resolution velocity field is a bit overwhelming, so for illustration purposes polygons were defined around each of the two bands of deep flow discussed herein and the vectors within those polygons were colored to highlight the predominant flow of interest for the present discussion. In the boundary current polygon, the grid cells where the meridional velocity is negative (southward) were highlighted in red. In the polygon for the interior pathway, grid cells where the zonal

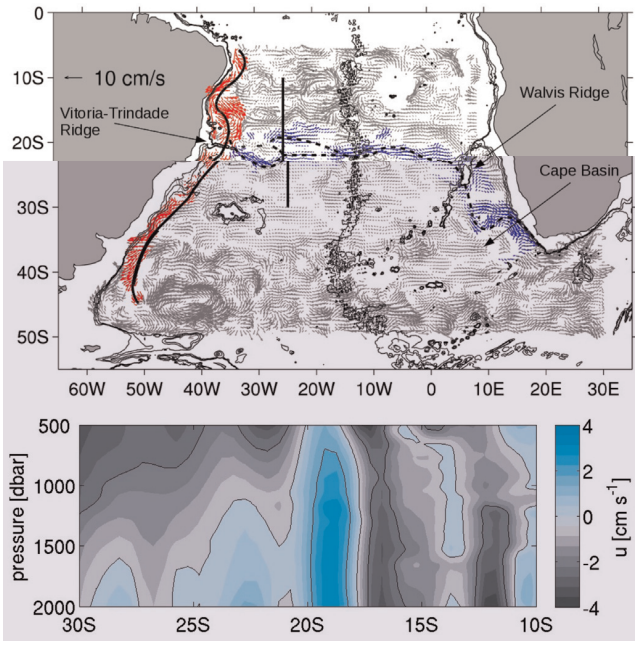

Fig. 3. Top panel: Velocity field at 2000 dbar derived from the Argo data. Red vectors highlight the southward to southwestward flow along the western boundary; blue indicates the eastward velocity originating near the Vitória-Trindade ridge. Isobaths: 2000, 2500 and 3000 m. Solid curves highlight the pathway of the DWBC along the South American coast. Dashed lines indicate regions where the pathway is less well defined as it moves to the interior of the basin. The meridional line indicates the location of the vertical section displayed in the lower panel. Areas with no vectors or shading indicate that velocities are too small to be significant with respect to a 95% confidence interval. Lower panel: Meridional-vertical structure of the eastward pathway in the top panel showing the zonal velocity in cm s^{-1} along 25°W from 10 to 30°S.

velocity is positive (eastward) were highlighted in blue. In order to provide a measure of the significance of the velocity field, a *t*-test is applied to detect which zonal velocity component is too small to be significant with respect to a 95% confidence interval. Vectors where the zonal component of the velocity fails this criteria are excluded from the top panel of Fig. 3. A similar *t*-test has also been applied to the meridional velocity component to ensure that the southward flows along the western boundary are significant. This was found to be the case with the exception of a very small band about 37°S, where the influence of the Brazil Malvinas confluence is large and the flow near the boundary has a relatively large (and significant) zonal component.

South of the Vitória-Trindade Ridge (Fig. 3, top panel), two branches of the flow are evident. The dominant branch is a strong southward flow (highlighted in red) along the coast of South America. This flow separates from the boundary at 38°S, the region of the Brazil–Malvinas Confluence, and continues southward all the way to 45°S. The Argo velocities also show eastward flow into the interior along roughly 22°S consistent with the spreading of the NADW towards the center of the basin; this signal is not as clear as the southward flow, however it is strongly supported by the CFC data (Fig. 2). Some details of the meridional and vertical structure of the eastward flow along this pathway (highlighted in blue) are given in Fig. 3 (bottom panel) which shows the zonal velocity in cm sec-1 obtained from the Argo product along 25°W from 10 to 30°S. The figure shows the evidence of two eastward jets at this longitude between 18 and 25°S. A jet with a higher eastward velocity (maximum of 3.4 cm s^{-1} at 2000 m) is observed between 18°S and 20°S while the second eastward jet to the south of it, between 21°S and 24°S, is observed to have a maximum eastward velocity of 1.7 cm s^{-1} at 2000 m at 22.5°S. These two eastward jets are located in the region where the CLIVAR water properties indicate the presence of NADW crossing 25°W (Fig. 2). The analysis also shows two westward flows at around 12° and 16°S, the southern one possibly representing part of a recirculation that may result in enhanced mixing of waters on this pathway. Also there is a very weak indication (at around 19°S, 8°W) of a northward transport that may feed back a small potion of the water into these westward flows (Fig. 3 top panel). However this small pathway is not connected by significant vectors and as such it is not clear how it fits in the overall circulation pattern. Nevertheless it appears that most of the significant flow continues towards the east. Eastward of the Walvis Ridge (~ 0°E), the Argo velocity product does not show a clear picture of a continuous jet (Fig. 3, top panel). This may be likely due to the high mesoscale motion in and northwest of the Cape Basin.

3. The Ocean General Circulation Model for the Earth Simulator (OFES)

Even with the improved data sets currently available for this study (updated hydrographic data, Argo float drift velocities), the data that can be used to study NADW pathways in the South Atlantic is still fairly limited. As such, a high quality ocean model can provide valuable circulation information. OFES is a massively parallelized implementation of version 3 of the NOAA/GFDL Modular Ocean Model (MOM3) run by the Japan Agency for Marine-Earth Science and Technology (JAMSTEC). The model equations have been discretized on a Mercator B grid with a horizontal resolution of 0.1° and 54 vertical z-levels. The simulation used in this study was spun up for 50 years with a monthly climatology of atmospheric forcing derived from the National Center for Environmental Prediction–National Center for Atmospheric Research (NCEP–NCAR) reanalysis (Masumoto et al., 2004), and then forced with daily mean NCEP–NCAR reanalysis data from January 1950 to December 2006 (Sasaki et al., 2008). OFES fields are publically available for a 27-year time period from January 1980 to December 2006 as snapshots at 3-day intervals. OFES reproduces the large-scale sea surface height variability in the South Atlantic well when compared to altimetric data (e.g., Dong et al., 2011; Perez et al., 2011). It has recently been used in various studies aimed at characterizing the time-mean and time-variability of components of the AMOC in the South Atlantic (e.g. Dong et al., 2011; Perez et al., 2011, van Sebille et al., 2012).

The OFES model has been validated in different regions of the global ocean by different authors (Masumoto, 2010, and references therein). In the context of NADW pathways in the South Atlantic, van Sebille et al. (2012) validated the velocity fields at the western boundary of the South Atlantic between 5°S and 11°S by comparing sections of 27-year mean meridional velocity in OFES in the DWBC with data collected by moored current meters (Schott et al., 2005) and, at 30°S with data from Lagrangian floats collected by Hogg and Thurnherr (2005). They concluded that the extent, position, and strength of the DWBC in OFES at these locations compare well with the available *in situ* observations at that time.

In the present study, further validation is done by comparing fields from the OFES model with hydrographic data collected on zonal sections along 5°S and 30°S, and the model output is also compared to the gridded World Ocean Atlas 2009 temperature and salinity climatology (WOA09; Locarnini et al., 2010), and the Argo data product discussed earlier (Section 2.2). These data were used to validate the accuracy of the location of the different water masses in the South Atlantic in the model and the total volume transport of NADW that enters and exits the South Atlantic at various latitudes between 4.6°S and 35°S.

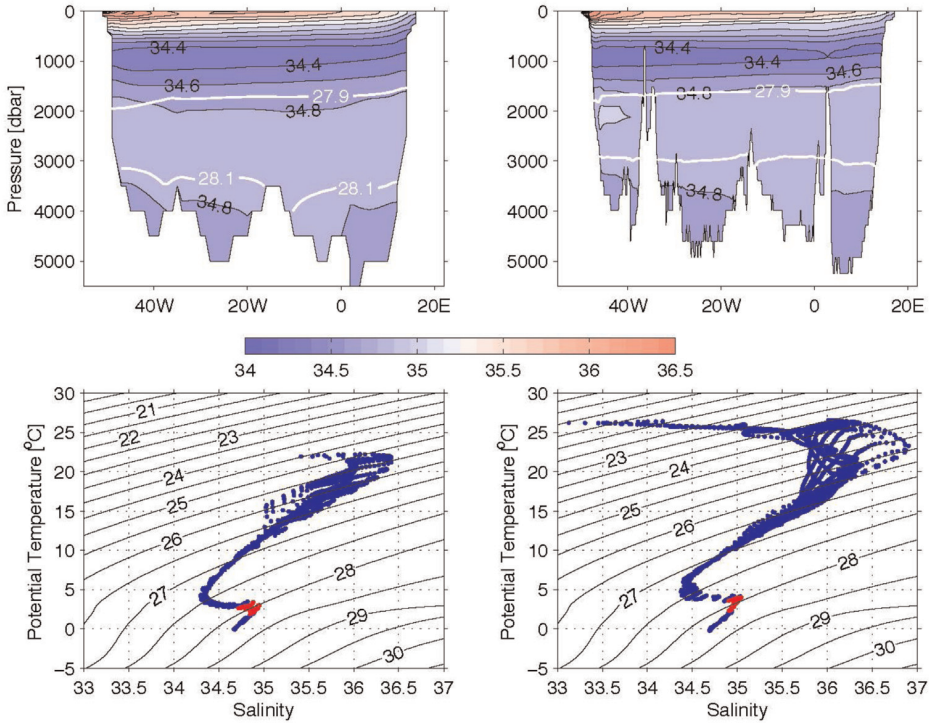

Fig. 4. Top panels: zonal sections of the climatological mean salinity from World Ocean Atlas 2009 (WOA09, left), and from the 27-year mean OFES model section (right), both along 30 °S. White color contours in the upper panels indicate neutral density levels 27.9 and 28.1 kg m^{-3}. The lower panels show the corresponding potential temperature/salinity diagrams from the WOA09 (left) and the model (right). Black contous indicate neutral density. Red indicates temperature and salinity values corresponding to the characteristics of the NADW (neutral densities 27.9 and 28.1 kg m^{-3}).

Comparisons of WOA09 and OFES salinity sections in the South Atlantic show that the boundaries of the neutral density levels (27.9 and 28.1 kg m^{-3}), which bracket the NADW, are very similar in the model and in the observations. An example is Fig. 4, which shows zonal sections of the climatological mean salinity from the WOA09 (left), and from the 27-year mean OFES model section (right), both along 30°S. The lower panel of Fig. 4 shows the corresponding potential temperature/salinity diagram. In the interior of the basin, the upper boundary of the NADW (neutral density 27.9) is at 1700 m both in the model and the observations. Near the continental boundaries, the upper boundary of the NADW is slightly deeper in the observations (2000 m in the west and 1500 m in the east for the observations, compared with 1800 m and 1500 m for the model) (Fig. 4 upper panel). Differences in the depth of the lower boundary of NADW (neutral density 28.1 kg m^{-3}) in the observations and the model are mostly related to differences in their representations of bottom topography in particular at the Mid Atlantic Ridge (deeper white contours in Fig. 4, upper panels). In addition, while the high salinity water on the eastern side in the observations is captured well in the model, the agreement is not as good in the west. The area bounded by the $S=34.8$ contour in the west is thicker in the observations than in the model. A potential temperature–salinity (T/S) comparison (Fig. 4, lower panels) indicates that at 30°S the model is more saline (35.1) than the observations (34.8) for upper NADW with neutral density between 27.9 and 28 kg m^{-3}, but with overall similar T/S structure along the 28.1 kg m^{-3} neutral density contour.

3.1. Lagrangian analysis

As mentioned in the Introducion, van Sebille et al. (2012) examined the pathways of NADW in the South Atlantic in the OFES model using Lagrangian pathways. In their experiment, van Sebille et al. (2012) focused their analysis on the connectivity between the DWBC and the Cape Basin.

In this paper, we used the simulated float database produced by van Sebille et al. (2012) to further examine the primary NADW pathway in the DWBC along the South American coast as well as the interior pathway. A brief description of the procedure they used is as follows: Float deployments were simulated along a grid at 5°S whenever the local instantaneous transport within the grid cell is southward. The grid spanned the full width of the South Atlantic between 1000 m and 3500 m depth and had 100 m vertical spacing. Since most southward transport is carried by the DWBC, the horizontal grid spacing was 0.1° in the DWBC west of 34°W and 0.5° in the rest of the basin. For a total of 5 years, one simulated float was released every 3 days. The vast majority of these floats are within the NADW layer (van Sebille et al., 2012). Each float was assigned a transport equal to the volume flux (velocity times area) through the grid cell in which it starts. After release, the floats were tracked forward with a fourth order Runge–Kutta integration scheme as implemented in the Connectivity Modeling System (CMS, Paris et al., 2013) using snapshots of the OFES velocity fields with 3-day resolution. Advection of a float was terminated when the float rises above 500 m depth, or when the float left the region bounded on the north by 5°S, at the south by 45°S, and on the east by 17°E. At the end of the 27-year run, the model output was looped to produce a longer time series (300 years) for forward integration of the simulated float tracks.

In this section, these 100,000+ synthetic float tracks are further analyzed to show the main pathway of the NADW along the continental slope of South America as well as the interior pathway indicated by hydrographic, tracers, and Argo observations discussed in Section 2. Transport estimates indicate that approximately 13.2 Sv (with a standard deviation of 3.1 Sv) are carried

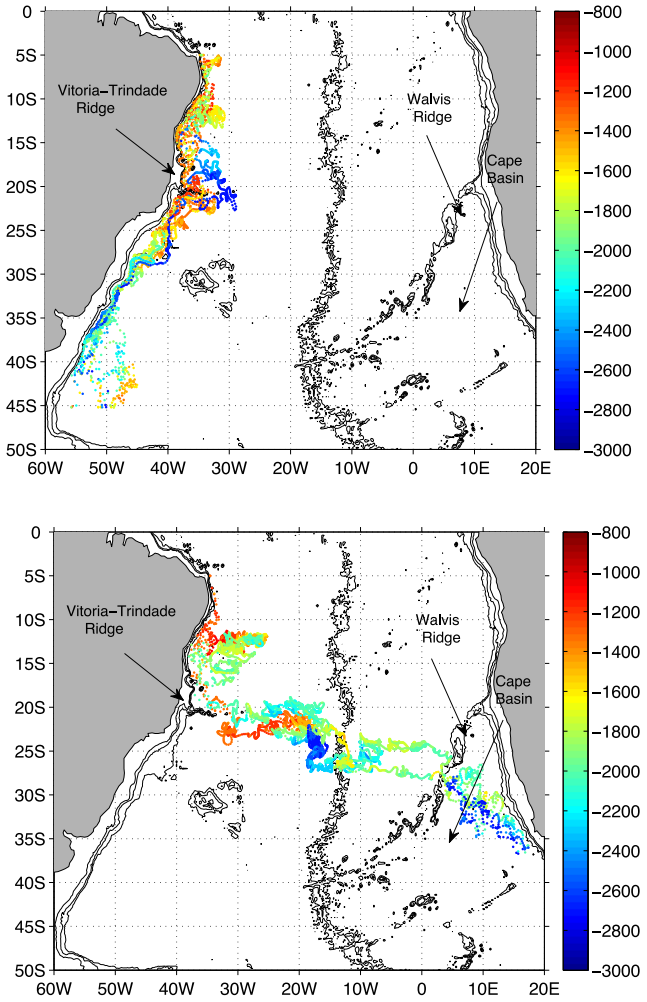

Fig. 5. Some examples of the two main pathways for synthetic floats launched in the NADW layer at 5°S west of 30°W. Top panel: Floats that follow the western boundary, defined as floats that cross 30°S west of 40°W and leave the South Atlantic across 45°S. Bottom panel: Floats that follow an interior pathway by leaving the South Atlantic across 17°E after having passed through a box defined by 9–10°W and 20–30°S. The color shading indicates the depth of the float in meters.

southward of 5 °S across the entire basin in the depth range where the float were deployed (1000–3500 m). This result is in agreement with the value obtained from the hydrographic data collected along the WOCE A07 line (12.6 Sv southward between neutral densities 27.9–28.1 kg m^{-3}, see Section 4). Lagrangian particle backtracking (i.e. tracing particle pathways backward in time to determine where the trajectories started) from points further south indicates that most of this south-southeastward flow originates west of 30°W along 5°S (90% of the total virtual floats).

The synthetic float trajectories illustrate the very eddy-rich nature of the flows in the South Atlantic. To focus on the primary pathways, the trajectories of the synthetic floats that cross 5°S are then followed for two different pathways. In the first pathway, the Lagrangian flow that crosses 30°S west of 30°W and continues south west of 40°W is tracked and the transport is estimated. Examples of some of the floats that follow this pathway are shown in Fig. 5, top panel. The total transport carried by those trajectories estimated following the procedure outlined in van Sebille et al. (2012) is approximately 9.4 Sv (with a standard deviation of 4.2 Sv) or 71% of the total southward transport across 5°S. A second pathway is defined by synthetic floats crossing 5°S west of 30°W that continue towards the Cape Basin directly beneath the Agulhas Ring corridor, crossing 17°E with the constraint of previously passing through the region bounded by 20 and 30°S and by 10 and 9°W (examples shown in Fig. 5, bottom panel). This is the interior pathway observed by the hydrographic, tracers, and Argo observations. The transport associated with this pathway is approximately 2.9 Sv (with a standard deviation of 1.4 Sv). This is approximately 22% of the simulated float transport in the NADW. These estimates are in agreement with those previously obtained by van Sebille et al. (2012) who calculated that of the 15.0 Sv net southward transport crossing 5°S, almost all of which is in the NADW density range, 10.2 Sv leaves the South Atlantic across the southern boundary at 45°S. They also calculated that 3.6 Sv exits across the Agulhas section at 17°E with the remaining floats recirculating in the basin and staying in the domain for a very long time (more than 300 years).

The present analysis of the synthetic Lagrangian floats leads to the conclusion that the main pathway along which the NADW spreads into the South Atlantic is along the continental shelf of South America, in the southward DWBC. The second pathway crosses the Atlantic in agreement with that described by van Sebille at al. (2012) and with the observational findings presented in Section 2.

3.2. Eulerian analysis

In this present analysis, OFES fields are also analyzed using more traditional Eulerian methods that allow direct comparison with observations. The objective of the analysis is to quantify the associated Eulerian transports and to look at the variability of the NADW pathways at different levels in the model and compare and contrast the Eulerian results with the Lagrangian results.

3.2.1. Kinetic energy variability

In order to provide a better picture of the energy distribution and the characteristic of the flow, the mean velocity magnitude and eddy kinetic energy (EKE) in the model were calculated at different depths within the NADW layer: 1700 m (the upper boundary of NADW), 2500 m (the NADW core depth), and 3600 m (the lower boundary of NADW). Examples are shown for the two upper depths in Fig. 6. The top panels show the annual mean (model years 2001 to 2006) of the velocity magnitude at 1700 m (left) and 2500 m (right). The two bottom panels show the mean EKE at 1700 m (left) and at 2500 m (right). Note, although not shown, the distribution of velocity and EKE at 3600 m figures are similar to those at 2500 m.

The mean velocity magnitude (Fig. 6, top panels) shows a steady and strong DWBC flow following the continental shelf of South America at 1700 m depth from the equator down to the Vitória-Trindade Ridge. At 2500 m, the mean DWBC flow is weaker but still identifiable. This pattern is in agreement with the mean Argo horizontal velocity map (Fig. 3). Analysis of the EKE fields (lower panels) reveals that the very energetic flow variability entering the South Atlantic from the tropics is fairly tightly confined along the western boundary (e.g. near 5°S). Traveling southward, the region of flow variability extends a little further offshore beginning around 8°S. This increase in the EKE is consistent with the DWBC breaking up into rings at this latitude as previously suggested by Dengler et al. (2004) and Schott et al. (2005). When this flow reaches the Vitória-Trindade Ridge at approximately 20°S the region of high variability stretches even further offshore, which is consistent with the flow becoming even more energetically eddy-dominated due to the interaction with the coastline and topographic ridge extending offshore.

There is a signature of enhanced EKE stretching eastward

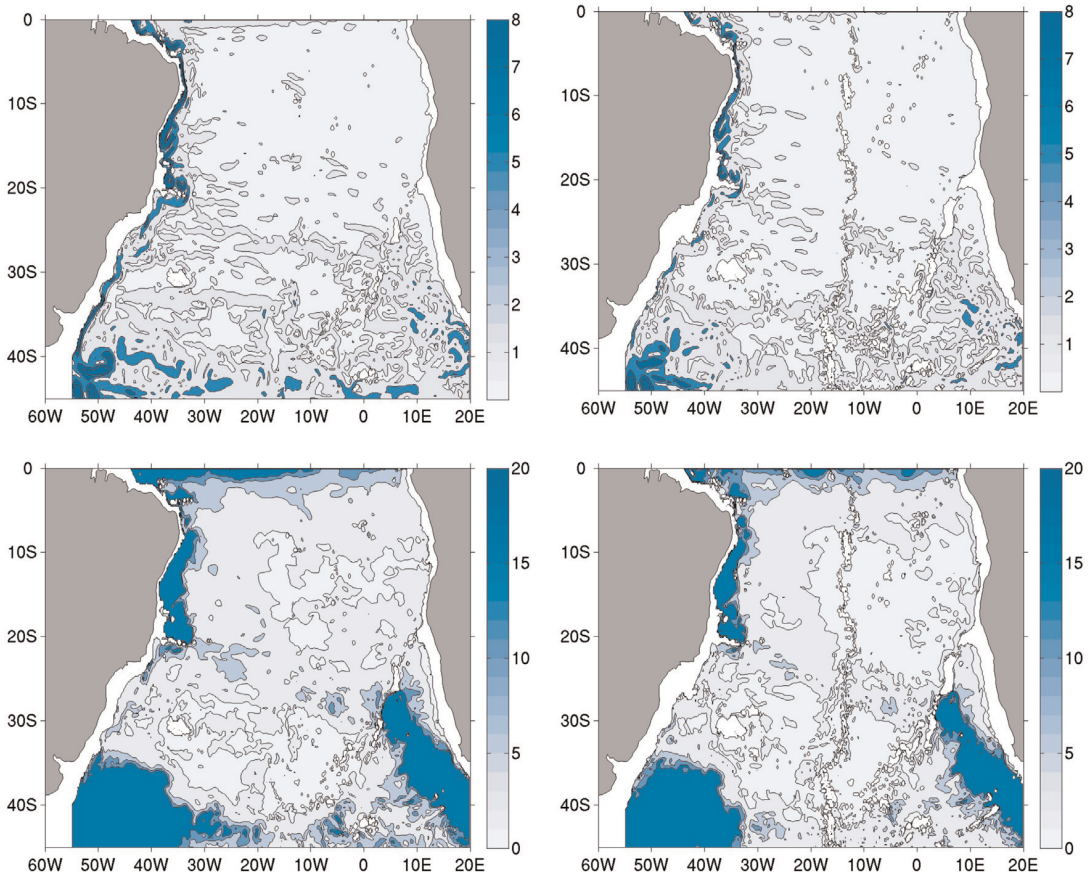

Fig. 6. Mean velocity magnitude in cm s^{-1} (top panels) and eddy kinetic energy (EKE) in cm^2 s^{-2} (bottom panels) calculated from the 2001 to 2006 OFES fields for two different depths: the upper boundary of the DWBC (1700 m, left) and the core of the DWBC (2500 m, right). Color bars are velocity magnitude in cm s^{-1} (top panels) and eddy kinetic energy (EKE) in cm^2 s^{-2} (bottom panels).

across the basin towards the Walvis Ridge (Fig. 6, bottom panels), suggesting that these eddies may play a role in transporting NADW into the interior (consistent with the simulated Lagrangian pathways, the Argo velocity map, and the water mass maps). This feature is most clearly seen in the EKE maps at 1700 m, although there are hints at 2500 m as well. The EKE maps also show a narrow tongue of higher variability close to the southern side of the Vitória-Trindade Ridge and continental slope to the south, consistent with a more stable and stationary DWBC flow reforming on the continental slope moving southward to about 25°S. This is confirmed by an increase in the mean horizontal velocity (top panels) south of 25°S that remains confined along the western boundary until 40°S (again the signals are stronger at 1700 m than 2500 m). High levels of energy are also observed at the eastern side of the basin in the region of the retroflection of the Agulhas Current and the Agulhas Ring corridor (blue area in bottom panels of Fig. 6 extending northwest from the southern tip of Africa), and in the western side of the basin at the confluence of the Brazil/Malvinas currents (blue area south of about 38°S near the western boundary). At the core of the NADW, 2500 m (Fig. 6 lower right panel), the EKE along the western boundary is lower than at 1700 m, but the western boundary signals are still much higher than is found in the interior. At the lower boundary of the NADW, 3600 m (not shown), the fields are less energetic than at 2500 m (Fig. 6), however, the distribution of EKE is similar.

Animations of the flows in the South Atlantic at all three levels analyzed in the model (not shown) indicate that energetic mesoscale features propagating westward are prevalent in the South Atlantic basin at these depths. In particular, signals generated in the Agulhas Current region propagate northwestward into the interior along the model ring corridor and in some cases reach the western boundary. To look at the westward component of the propagation of the mesoscale signals in the basin, speed and EKE were plotted as a function of longitude for different latitudes and at different depths. An example of this westward propagation can be seen in Fig. 7 that shows a Hovmoller diagram of the speed and the EKE along 25°S at 2500 m from 2001 to 2006 as a function of longitude and time. The observed westward propagation has the characteristics of a Rossby wave-like feature with estimated speeds of about 5–7 cm/s. The feature is consistent with previous satellite and *in situ* observations of first baroclinic mode Rossby waves (e.g., Osychny and Cornillon, 2004; Meinen and Garzoli, 2014).

3.2.2. *Volume transports*

During WOCE, a hydrographic section was occupied along 4.6°S (A07; Oudot, 1993; Fajar et al., 2011). This latitude is close to the latitude of the simulated float deployments in the experiment by van Sebille et al. (2012) discussed in Section 3.1. Data from the WOCE section is used to obtain additional Eulerian validation of the OFES model flow crossing this latitude, particularly within NADW density levels. Temperature and salinity data from the WOCE section are used in conjunction with Argo drift velocities, at nominally 1000 m depth, to calculate the absolute volume transport of NADW between neutral density levels. From the temperature and salinity profiles, the geostrophic velocities are

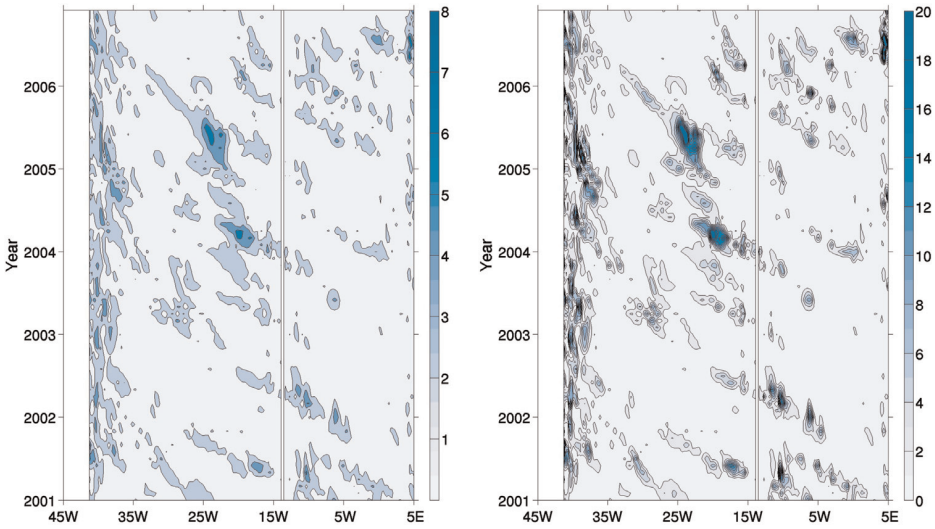

Fig. 7. Hovmoller diagrams of the horizontal velocity magnitude in cm s^{-1} (left) and eddy kinetic energy (EKE) in $cm^2\ s^{-2}$ (right) calculated from the 2001 to 2006 OFES fields across 25°S and at 2500 m depth, as a function of longitude and time. Color bars are velocity magnitude in cm s^{-1} (left) and eddy kinetic energy (EKE) in $cm^2\ s^{-2}$ (right). The vertical line at approximately 14°W indicate no data due to the presence of the Mid Atlantic Ridge.

calculated with a reference level of 1000 m. Using the 3-D velocity profiles derived from Argo in the South Atlantic (Section 2.2), the absolute velocity at 1000 m between each pair of hydrographic sections is added to the geostrophic relative velocities in order to obtain the absolute velocity. From the latter, the total integrated NADW transport across the basin-wide section is estimated to be −12.6 Sv (southward) between neutral density layers 27.9 and 28.1 kg m^{-3}. The corresponding mean transport in the OFES model across 5°S between neutral densities 27.9 and 28.1 kg m^{-3} is −13.9 Sv (southward). The standard deviation (σ) of the mean values obtained from the 27-year model output is 0.95 Sv. This total integrated southward flow is mostly concentrated west of 30°W.

From the model velocity fields, meridional volume transports at different latitudes are obtained between neutral density levels 27.9 and 28.1 kg m^{-3} corresponding to the boundaries of the NADW. Results focusing on the meridional transport along the western and eastern boundaries are summarized in Fig. 8 and Table 1. West of 30°W, there is a southward flow of −13.9 Sv (σ=1.2 Sv) at 10°S that is reduced to −11.8 Sv (σ=0.7 Sv) at 20°S, the latitude of the Vitória-Trindade Ridge. Between 20°S and 30°S, the coastline makes an abrupt shift westward of roughly 5° of longitude, so south of 25°S different integration limits were used. The strong southward mean flow continues to be concentrated on the western boundary following the continental shelf of South America. From the −12 Sv flowing southward at 25°S, −9.0 Sv (σ=0.5 Sv) can be found concentrated west of 40°W (as shown in Fig. 8) while a smaller −2.5 Sv is flowing south more broadly between 30°W and 40°W (not shown in the figure for visual impact). The southward transport at 35°S is −7.5 Sv (σ=0.3 Sv) and there is little indication of additional southward flow offshore of 40°W. The loss of transport between 30°S and 35°S seems to be primarily associated with a significant recirculation offshore of the DWBC. Analysis of the model zonal velocity shows that the mean zonal transport is westward −1.3 Sv at 30°S and increase to −3.0 Sv at 35°S which is an indication of the recirculation consistent with the velocity field from the Argo floats shown in Fig. 3. Detailed analysis of the model (not shown) indicates that by 35°S, there is a northward volume transport of 1.5 Sv between 45°W and 40°W, or roughly 20% of the strength of the southward DWBC transport at that latitude.

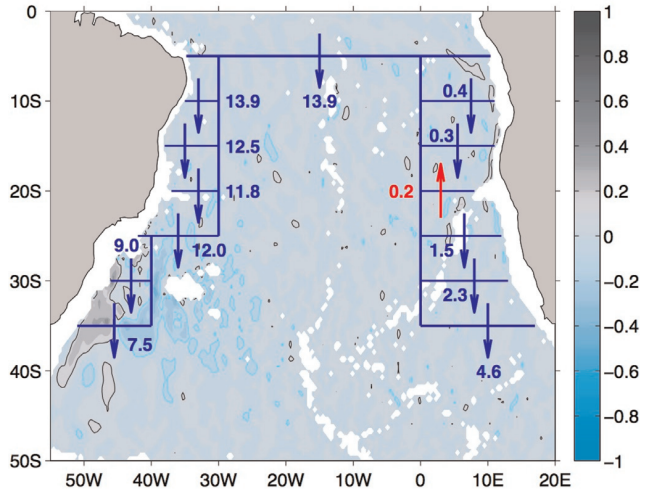

Fig. 8. Volume transports between neutral density levels 27.9 and 28.1 kg m^{-3} corresponding to NADW, and obtained from the OFES velocity fields. At 5°S the transport is integrated across the basin. At other latitudes, transports are calculated west of 30°W (from 5 to 25°S) and west of 40°W at 30° and 35°S. At the eastern side of the ocean, volume transports are calculated east of 0°E. The color shading show the zero-lag correlation between meridional velocity in the South Atlantic at a depth of 2500 m with the DWBC meridional volume transport along 34.5°S. The color scale is the correlation value from 1.0 to −1.0. Black and cyan contours show positive and negative correlations that are significant with 95% confidence.

Along the eastern boundary, east of 0°E, only a very small volume of water crosses 5°S (−0.2 Sv with a standard deviation of 0.03 Sv) and the meridional volume transport near the eastern boundary remains small with values of −0.4 (σ=0.01 Sv) at 10°S and 0.2 Sv at 20°S (σ=0.03 Sv). At 25°S, the contributions from the interior of the basin begin to augment the southward volume transport, reaching a maximum of −4.6 Sv (σ=0.2 Sv) at 35°S.

Fig. 8 can also be used to revisit a concept discussed earlier, namely that the DWBC reforms in a coherent manner as a continuous boundary current south of the Vitória-Trindade ridge at 20°S. To illustrate this, the zero-lag correlations between the DWBC meridional volume transport at 34.5°S integrated from

Table 1
Meridional volume transport in Sv (1 Sv = 10^6 m^3 s^{-1}, negative indicates southward), Numbers in parentheses correspond to the standard deviation. Observed values (red) were obtained from: CTD and Argo observations at 5°S, CTD observations at 30°S, XBT observations combined with CTD and Argo floats data at ~35°S, and a line of PIES (pressure-equipped inverted echo sounder) moorings along 34.5°S. See text for more details. Column 1: Eulerian transports estimated from the OFES velocity field between neutral densities 27.9 and 28.1 kg m^{-3} (black) and from observations (red) between the same density levels. Column 2: Eulerian transports estimated from the OFES velocity field between 1000 and 3500 m (black) and from observations (red) between the same levels. Column 3: Lagrangian transports estimated from the simulated float trajectory field for floats deployed between 1000 and 3500 m.

	Eulerian transports estimated between neutral density surfaces 27.9–28.1 (~1700–3000 m)	**Eulerian transports estimated between depth surfaces 1000–3500 m**	**Lagrangian transports estimated from simulated floats deployed between depths of 1000–3500 m**
From model results from coast to coast at 5°S.	**−13.9 Sv (0.96)**	**−16.8 Sv (1.1)**	**−13.2 Sv (3.2)**
From CTD and Argo observations from coast to coast at 5°S	**−12.6 Sv**	**−21.4 Sv**	**n/a**
	From 40.0°W to the west coast	**From 40.0°W to the west coast**	**From 40.0°W to the west coast**
Model results at 34.5°S	**−7.5 Sv (0.3)**	**−16.4 Sv (0.6)**	**−9.4 Sv (4.2)**
From CTD observations at 30°S	**−8.2 Sv**	**−14.5 Sv**	**n/a**
From combined observations at ~35°S	**−9.0 Sv (3.1)**	**−19.5 Sv (5.4)**	**n/a**
	From 0°E to east coast	**From 0°E to east coast**	**From 0°E to east coast**
Model results at 34.5°S	**−4.6 Sv (0.2)**	**−3.0 Sv (1.4)**	
From combined observations at ~35°S	−4.2 **Sv** (1.9)	−3.7 **Sv** (1.0)	n/a

coast to 44.5°W and 1700 m to 3000 m (over the 27-year record) and the meridional velocity at 2500 m depth were determined at each OFES grid-point in the South Atlantic (color shading in Fig. 8). Correlations are significant with 95% confidence, if they are larger than ±0.11 (assuming there are 12 independent samples per year over 27 years, or 324 independent samples indicated with black and gray contours). Positive correlations (gray shading) along the coast between roughly 22°S and 42°S indicate that the meridional flow between these latitudes is coherent with the DWBC at 34.5°S. This is consistent with the DWBC having reformed into a steady flow in this region, as opposed to the eddy dominated flow where the horizontal scales would be small enough that transport would be poorly correlated beyond an eddy length scale. The negative correlations (cyan shading) observed offshore of the strong positive correlation band are consistent with recirculation of the DWBC waters in the model between roughly 37°S to 22°S, just south of the Vitória-Trindade ridge. Note that the pattern of the zero-lag correlations is not significantly different from that of the maximum lagged correlations (not shown).

In what follows, Eulerian volume transports obtained from the OFES model and available observations across the basin and at the boundaries are analyzed at 5°S, 30°S, and 34.5°S and compared with the Lagrangian transports estimated by van Sebille et al. (2012). Estimates of the Eulerian volume transports are computed in two ways: integrated within the neutral density range 27.9 and 28.1 kg m^{-3}, the defined boundaries of NADW; and integrated between 1000 and 3500 m, the depth span over which the synthetic Lagrangian floats were launched by van Sebille et al. (2012). Results are shown in Table 1; negative numbers indicate southward flow. Column 1 (black numbers) are the Eulerian transports estimated from the OFES model between density levels 27.9–28.1 kg m^{-3}. In the same column results are compared with estimates previously discussed obtained from WOCE A07 CTD data coupled with Argo data collected along nominally 5°S, and with those obtained by other observational systems in the area: from a CLIVAR A10 CTD section collected along 30°S, and from the average of the values obtained from a series of expendable bathythermograph (XBT) transects conducted nominally along 35°S and analyzed jointly with hydrographic and Argo data (see Garzoli et al., 2013) (called "combined observations" in the Table). Column 2 show the volume transports estimated from 1000 to 3500 m in a Eulerian reference frame, and column 3 the Lagrangian transports from simulated floats deployed between 1000 and 3500 m following van Sebille et al. (2012). Overall, there is agreement between model results and observations. Across 5°S basin-wide, there is very good agreement between the basin wide transports determined between neutral densities 27.9 and 28.1 kg m^{-3} (−13.9 Sv, σ=0.96 from the model, −12.6 Sv from observations). The simulated Lagrangian estimate of the flow at 5°S in the 1000–3500 m layer (−13.2 Sv, σ=3.2 Sv) is similar to the Eulerian simulated transport between neutral density levels (13.9 Sv, σ=0.96 Sv). However, the Eulerian estimates from observations between 1000 and 3500 m (−21.4 Sv) are noticeably larger than those obtained from the model (−16.8 Sv, σ=1.1 Sv); this could be an indication of the model not capturing the circulation in the deep ocean (below 3000 m) correctly.

When transports are estimated west of 40°W there is very good agreement between estimates from the model and the observations. The difference between Eulerian and Lagrangian results can be explained by analyzing the depth of the simulated float trajectories, which suggests that even though the synthetic floats were launched between 1000 and 3500 m, the majority of the floats tended to occupy a more restricted depth range from 1000 to less than 3000 m.

At the eastern boundary there is good agreement between the model and observations in Eulerian coordinates (Table 1), but the relationship is the opposite of those observed near the western boundary (see also Fig. 8). For example, southward volume transport across 34.5°S and east of 0°E in the model is larger when estimated between density layers (−4.6 Sv, σ= 0.2 Sv) than between 1000 and 3500 m (−2.8 Sv, σ=0.23 Sv); a similar, albeit smaller, difference is found in the observations (−4.2 Sv, σ=1.9 Sv versus −3.7 Sv, σ=1.0 Sv). This is because at the eastern boundary the fixed 1000–3500 m depth range includes some of the northward flow of Antarctic Intermediate Water (AAIW) above the NADW, and the result is a smaller net southward flow in the fixed depth integral (e.g., Schmid et al., 2003).

In addition to the comparisons shown in the table, one additional data set that can be compared is from the pressure-equipped inverted echo sounders (PIES) deployed along 34.5°S west of 44.5°W (Meinen et al., 2012). The PIES transports calculated between density levels 27.9 and 28.1 kg m^{-3} (−10.9 Sv) is larger than the model result (−5.7 Sv, not shown in the table) when integrated to 44.5°W. About 2 Sv of this difference can be

explained by a northward flow observed in the model, between 47°W and 49°W that is not present in the PIES observations. Furthermore the agreement improves when the volume transports are calculated between 1000 and 3500 m (PIES: −16.7 Sv; model: −14.0 Sv).

4. Discussion and conclusions

Lagrangian and Eulerian analysis of the OFES model, validated against hydrographic/tracer, XBT, Argo and PIES data, provides a description of the pathways of the DWBC as it flows through the South Atlantic, carrying NADW southward as the lower limb of the AMOC. From the Eulerian model analysis, it is estimated that approximately −13.9 Sv of water crosses 5°S flowing southward into the South Atlantic in a layer limited by the neutral density surfaces 27.9 and 28.1 kg m^{-3}. These density levels correspond approximately to depths between 1700 m and 3000 m, and are the boundaries of the NADW ventilated with CFCs in the South Atlantic.

Re-analysis of the WOCE-era hydrographic data collected along 5°S in conjunction with the Argo drift velocity field is in agreement with further analysis of the Lagrangian floats advected for 300 years in OFES model following van Sebille et al. (2012). This analysis indicates that 90% of the total floats that constitute the southward flow at 5°S originate west of 30°W. These results are obtained by backtracking the particles, and by the Eulerian estimates of volume transport integrated across 5°S.

Crossing 5°S and mostly concentrated west of 30°W, the DWBC carries NADW along the coast of South America and, in the model in agreement with previous results, breaks up into rings near 8°S, a region where the flow is mostly "non-steady." Analyses of the eddy kinetic energy (EKE) at different depth levels in the model indicate high levels of energy spreading further offshore south of 8°S, consistent with the formation of energetic rings. This "ring-dominated" flow continues southward to the Vitória-Trindade Ridge (near 20°S). When the ring-dominated flow reaches the Vitória-Trindade Ridge, the NADW is forced to flow to the east due to the topography. The branching of the flow in this area is due to the preservation of potential vorticity (Zangenberg and Siedler, 1998). Theory suggests that part of the along-slope southward flow turns into a zonal flow to the east at the latitudes where the change in planetary vorticity is sufficiently large to compensate for the change in potential vorticity due to the initial depth changes. In the Southern Hemisphere, the Coriolis parameter is negative and the water column rotates clockwise with increasing depth.

The model suggests that about 22% of the NADW flows eastward from the western boundary into the interior South Atlantic. WOCE and CLIVAR-era CFC observations give a clear pathway eastward roughly underlying the Agulhas Ring corridor, and extending over a fairly broad latitude range (Figs. 1 and 2). The Argo velocity field in the upper NADW layer does not indicate a robust mean pathway for this eastward flow; rather it is characterized by several meanders (Fig. 3) and relatively weak mean eastward jets. As there is a broad latitudinal distribution of properties extending eastward into the interior and the complex Argo velocity mean picture is not particularly suggestive of a narrow corridor of NADW transfer under the Agulhas Ring corridor, it is possible that more than one mechanism is involved in the transfer of ventilated NADW properties to the east near 20°S. Therefore, it is hypothesized that this southeastward spreading of properties could result from a combination of the mechanism of eddy-thickness flux divergence due to Agulhas ring decay, previously proposed and examined by van Sebille et al. (2012), enhanced by the clearly highly energetic eddy field at the Vitória-Trindade ridge and eastward jets observed in the velocity field.

The most prevalent motion noted in the animations of the ocean model velocity fields at three depths (not shown, but this can be inferred from the connectivity of the elevated EKE regions in the Cape Basin to Vitoria-Trindade Ridge in Fig. 6, and Hovmoller diagrams in Fig. 7) associated with the upper boundary, core, and lower boundary of NADW is a strong northwestward propagation consistent with the westward propagation characteristics of Rossby Waves. It is hypothesized that this westward propagation interacting with the mean circulation field may be the reason why south of the Vitória-Trindade Ridge most of the flow (~71% in the model) returns to the continental slope, as a more steady flow, forming the main branch of the DWBC south of the ridge. However, a detailed analysis of this complicated eddy-mean flow interaction is beyond the scope of the present study and is a topic for future research.

At 34.5°S, the DWBC meridional volume transport between the coast and 44.5°W and from 1000 to 3500 m is about −14 Sv in the model. This model transport is close to an estimate of -14.5 Sv from hydrographic data collected at 30°S. Further analysis of the model trajectories (not shown) indicates that after crossing 34.5°S, a small amount (about 1 Sv) of NADW flows towards the east at the latitude where the Malvinas Current turns offshore (~38°S), in agreement with previous results from van Sebille et al. (2012). The rest of the flow continues south to approximately 45°S where it joins with the eastward flowing Antarctic Circumpolar Current.

Eulerian volume transport estimates obtained from the velocity field of the OFES model between 27.9 and 28.1 neutral density levels (Fig. 8) indicate that about 2 Sv of NADW does not leave the South Atlantic as NADW. This is consistent with previous modeling and observational results (Garzoli and Matano, 2011), which found that in the Brazil–Malvinas Confluence region approximately 2.6 Sv of water is transformed from NADW to AAIW.

Based on the available observations and the model analysis, we conclude that the NADW follows two different pathways south of 5°S. The main pathway (~71%) is southward in the DWBC flowing along the coast of South America. A smaller portion (~22%) flows eastward towards the interior of the basin. Better understanding of the pathways of the lower limb of the AMOC will be crucial for quantifying the fluxes of heat, fresh water and CO_2 through the South Atlantic. Furthermore, for understanding variations of the AMOC, detailed knowledge of temporal changes of the pathways as well as what mechanisms control those variations will be necessary.

Acknowledgments

This research was carried out in part under the auspices of the Cooperative Institute for Marine and Atmospheric Studies (CIMAS), a Cooperative Institute of the University of Miami and the National Oceanic and Atmospheric Administration (NOAA), cooperative agreement #NA10OAR4320143. Additional support was provided by NOAA's Climate Program Office under Grant # NA13OAR4310131, by the NOAA Southwest Atlantic MOC project, and the Physical Oceanography Division of NOAA's Atlantic Oceanographic and Meteorological Laboratory. Rana Fine thanks the Physical Oceanography Program of the National Science Foundation for support. Erik van Sebille was supported by the Australian Research Council via Grant DE130101336. The OFES simulation was conducted on the Earth Simulator under the support of JAMSTEC. The authors are indebted to Yoshikazu Sasai and Ricardo Matano for providing output from the OFES simulations. The authors would like the anonymous reviewers whose comments helped to the submission of an improved manuscript.

References

Arhan, M., Mercier, H., Park, Y.-H., 2003. On the deep water circulation of the eastern South Atlantic Ocean. Deep-Sea Res. I 50, 889–916. http://dx.doi.org/10.1016/S0967-0637(03)00072-4.

Bower, A.S., Lozier, M.S., Gary, S.F., Böning, C.W., 2009. Interior pathways of the North Atlantic meridional overturning circulation. Nature 459 (7244), 243–247.

Bryden, H.L., King, B.A., McCarthy, G.D., 2011. South Atlantic overturning circulation at 24°S. J. Mar. Res. 69 (1), 38–55.

CLS, 1996. AVISO User Handbook for Merged TOPEX/POSEIDON products CLS Ref.: AVI-NT-02-101. See ⟨http://www.aviso.altimetry.fr/en/data/product-information/aviso-user-handbooks.html⟩.

Dengler, M., Schott, F.A., Eden, C., Brandt, P., Fischer, J., Zantopp, R.J., 2004. Break-up of the Atlantic Deep Western Boundary Current into eddies at 8°S. Nature 432, 1018–1020.

Dong, S., Baringer, M., Goni, G., Garzoli, S., 2011. Importance of the assimilation of Argo Float Measurements on the Meridional Overturning Circulation in the South Atlantic. Geophys. Res. Lett. 38 (L18603). http://dx.doi.org/10.1029/2011GL048982.

Drijfhout, S.S., Weber, S.L., van der Swaluw, E., 2011. The stability of the MOC as diagnosed from model projections for pre-industrial, present and future climates. Clim. Dyn. 37, 1575–1586. http://dx.doi.org/10.1007/s00382-010-0930-z.

Fajar, N.M., Perez, F.F., Velo, A., Rios, A.F., 2011. Data Recovery of A06 and A07.

WOCE cruises. Earth Syst. Sci. Data Discuss. vol. 4, pp. 9–122 doi: 10.5194/essdd-4-99.

Fine, R.A., Molinari, R., 1988. A continuous Deep Western Boundary Current between Abaco (26.5°N) and Barbados (13°N). A Rapid Response Pap. Deep-Sea Res. 35, 1441–1450.

Fine, R.A., Rhein, M., Andrié, C., 2002. Using a CFC effective age to estimate propagation and storage of climate anomalies in the Deep Western North Atlantic Ocean. Geophys. Res. Lett. 29 (24), 2227. http://dx.doi.org/10.1029/2002GL015618.

Garzoli, S.L., Matano, R., 2011. The South Atlantic and the Atlantic Meridional Overturning Circulation. Deep-Sea Res. Part II 58 (17-18), 1837–1847. http://dx.doi.org/10.1016/j.dsr2.2010.10.063.

Garzoli, S.L., Baringer, M.O., Dong, S., Perez, R., Yao, Q., 2013. South Atlantic meridional fluxes. Deep-Sea Res. Part I 71, 21–32. http://dx.doi.org/10.1016/j.dsr.2012.09.003.

Hogg, N.G., Owens, W.B., 1999. Direct measurement of the deep circulation within the Brazil Basin. Deep-Sea Res. II 46, 335–353. http://dx.doi.org/10.1029/2004/JC002311.

Hogg, N.G., Thurnherr, A.M., 2005. A zonal pathway for NADW in the South Atlantic. J. Oceanogr. 61 (3), 493–507.

Johns, W.E., Beal, L.M., Baringer, M.O., Molina, J.R., Cunningham, S.A., Kanzow, T., Rayner, D., 2008. Variability of shallow and Deep Western Boundary Currents off the Bahamas during 2004-05: Results from the 26°N RAPID-MOC array. J. Phys. Oceanogr. **38**, 605–623.

Jullion, L., Heywood, K.J., Naveira Garabato, A.C., Stevens, D.P., 2010. Circulation and water mass modification in the Brazil–Malvinas confluence. J. Phys. Oceanogr. 40, 845–864. http://dx.doi.org/10.1175/2009JPO4174.1.

Kieke, D., Rhein, M., Stramma, L., Smethie Jr., W.M., Bullister, J.L., LeBel, D.A., 2007. Changes in the pool of Labrador Sea Water in the subpolar North Atlantic related to changes in the upper North Atlantic circulation Geophysical. Res. Lett. 34 (LO6605). http://dx.doi.org/10.1029/2006GL028959.

Koltermann, K.P., V.V.Gouretski and K.Jancke, 2011: Hydrographic Atlas of the World Ocean Circulation Experiment (WOCE). Volume 3: Atlantic Ocean (eds. M. Sparrow, P. Chapman and J. Gould). International WOCE Project Office, Southampton, UK, ISBN 090417557X.

Locarnini, R.A., Mishonov, A.V., Antonov, J.I., Boyer, T.P., Garcia, H.E., Baranova, O.K., Zweng, M.M., Johnson, D.R., 2010. World Ocean Atlas 2009. In: Levitus, Temperature S. (Ed.), NOAA Atlas NESDIS 68, vol. 1. U.S. Government Printing Office, Washington, DC, p. 184.

Lumpkin, R., Speer, K., 2007. Global ocean meridional overturning. J. Phys. Oceanogr. **37**, 2550–2562.

Masumoto, Y., Sasaki, H., Kagimoto, T., Komori, N., Ishida, A., Sasai, Y., Miyama, T., Motoi, T., Mitsudera, H., Takahashi, K., Sakuma, H., Yamagata, T., 2004. A fifty-year eddy-resolving simulation of the world ocean: preliminary outcomes of OFES (OGCM for the Earth Simulator). J. Earth Simul. 1, 35–56.

Masumoto, Y., 2010. Sharing the results of a high-resolution ocean general circulation model under a multi-discipline framework a review of OFES activities. Ocean Dyn. 60, 633–652.

Matano, R.P., Beier, E.J., 2003. A kinematic analysis of the Indian/Atlantic interocean exchange. Deep-Sea Res. II 50 (1), 229–249.

Meinen, C.S., Johns, W.E., Garzoli, S.L., van Sebille, E., Rayner, D., Kanzow, T., Baringer, M.O., 2012. Variability of the Deep Western Boundary Current at 26.5 °N during 2004-2009. Deep-Sea Res. Part II 85, 154–168. http://dx.doi.org/10.1016/j.dsr2.2012.07.036.

Meinen, C., Garzoli, S.L., 2014. Attribution of Deep Western Boundary Current variability at 26.5°N. Deep Sea Res. I 90, 81–90. http://dx.doi.org/10.1016/ j.dsr.2014.04.016.

Molinari, R.L., Fine, R.A., Wilson, W.D., Curry, R.G., Abell, J., McCartney, M.S., 1998. The arrival of recently formed Labrador Sea Water in the Deep Western Boundary Current at 26.5°N. Geophys. Res. Lett. 25, 2249–2252.

Müller, T.J., Ikeda, Y., Zangenberg, N., Nonato, L.V., 1998. Direct measurements of western boundary currents of Brazil between 20°S and 28°S. J. Geophys. Res. 103, 5429–5437.

Oudot, C., 2 January–10 February 1993. Total CO2 and total alkalinity data obtained during the R/V L'Atalante cruise in the Atlantic Ocean. WOCE Section A06. Carbon Dioxide Information Analysis Center, Oak Ridge National Laboratory, US Department of Energy, Oak Ridge, Tennessee A06 1993 1993 doi: 10.3334/CDIAC/otg.WOCE. ⟨http://cdiac.ornl.gov/ftp/oceans/a06woce/⟩.

Osychny, V., Cornillon, P., 2004. Properties of Rossby waves in the North Atlantic estimated from satellite data. J. Phys. Oceanogr. 34 (1), 61–76.

Paris, C., Helgers, J., van Sebille, E., Srinivasan, A., 2013. Connectivity Modeling System: a probabilistic modeling tool for the multi-scale tracking of biotic and abiotic variability in the ocean. Environ. Model. Softw. 42, 47–54.

Perez, R.C., Garzoli, S.L., Meinen, C.S., Matano, R.P., 2011. Geostrophic Velocity Measurement Techniques for the Meridional Overturning Circulation and Meridional Heat Transport in the South Atlantic. J. Atmos. Ocean. Tech. 28, 1504–1521.

Preu, B., Hernández-Molina, F.J., Violante, R., Piola, A.R., Paterlini, C.M., Schwenk, T., Voigt, I., Krastel, S., Speiss, V., 2013. Morphosedimentary and hydrographic features of the northern Argentine margin: the interplay between erosive, depositional and gravitational processes and its conceptual implications. Deep-Sea Res. I 75, 157–174. http://dx.doi.org/10.1016/j.dsr.2012.12.013.

Provost, C., Escoffier, C., Maamaatuaiahutapu, K., Kartavtseff, A., Garçon, V., 1999. J. Geophys. Res. 104, 21,033–21,049. http://dx.doi.org/10.1029/1999JC900049.

Reid, J.L., 1989. On the total geostrophic circulation of the South Atlantic Ocean: Flow patterns, tracers, and transports. Prog. Oceanogr. 23, 149–244.

Rimaud, J., Speich, S., Blanke, B., Grima, N., 2012. The exchange of Intermediate Water in the South East Atlantic: Water mass transformations diagnosed from the Lagrangian analysis of a regional ocean model. J. Geophys. Res. 117 (C08034). http://dx.doi.org/10.1029/2012JC008059.

Sasaki, H., Nonaka, M., Masumoto, Y., Sasai, Y., Uehara, H., Sakuma, H., 2008. An eddy-resolving hindcast simulation of the quasiglobal ocean from 1950 to 2003 on the Earth Simulator. In: Hamilton, K., Ohfuchi, W. (Eds.), High Resolution Numerical Modelling of the Atmosphere and Ocean. Springer, New York, pp. 157–185.

Schmid, C., Garraffo, Z.D., Johns, E., Garzoli, S.L., 2003. Pathways and Variability at intermediate depths in the tropical Atlantic. EOS 68, 233–268.

Schmid, C., 2014. Mean vertical and horizontal structure of the subtropical circulation in the South Atlantic from three-dimensional observed velocity fields. Deep-Sea Res. I 91 (9), 50–71. http://dx.doi.org/10.1016/j.dsr.2014.04.015.

Schmitz, W.J., McCartney, M.S., 1992. On the North Atlantic circulation. Rev. Geophys. 31, 29–50.

Schott, F.A., McCreary, J.P., Johnson, G.C., 2004. Shallow overturning circulations of the tropical-subtropical oceans. Earth climate: the ocean–atmosphere interaction. In: Wang, C., Xie, S.-P., Carton, J.A. (Eds.), Geophysical Monograph, American Geophysical Union, pp. 261–304.

Schott, F.A., Dengler, M., Zantopp, R.J., Stramma, L., Fischer, J., Brandt, P., 2005. The shallow and deep western boundary circulation of the South Atlantic at 5_–11_S. J. Phys. Oceanogr. 35, 2031–2053.

Speich, S., Blanke, B., Cai, W., 2007. Atlantic meridional overturning circulation and the Southern Hemisphere supergyre. Geophys. Res. Lett. 34, L23614. http://dx.doi.org/10.1029/2007GL031583.

Troupin, C., Barth, A., Sirjacobs, D., Ouberdous, M., Brankart, J.-M., Brasseur, P., Rixen, M., Alvera Azcarate, A., Belouni, M., Capet, A., Lenartz, F., Toussaint, M.-E., Beckers, J.-M., 2012. Generation of analysis and consistent error fields using the Data Interpolating Variational Analysis (Diva). Ocean Model. 52–53, 90–101.

van Sebille, E., Johns, W.E., Beal, L.M., 2012. Does the vorticity flux from Agulhas rings control the zonal pathway of NADW across the South Atlantic. J. Geophys. Res. 117, C05037. http://dx.doi.org/10.1029/2011JC007684.

Wanninkhof, R., Doney, S.C., Bullister, J.L., Levine, N.M., Warner, M., Gruber, N., 2010. Detecting anthropogenic CO_2 changes in the interior Atlantic Ocean between 1989 and 2005. J. Grophys. Res. 115, C11028. http://dx.doi.org/10.1029/2010JC006251.

Weiss, R.F., Bullister, J.L., Gammon, R.H., Warner, M.J., 1985. Atmospheric chlorofluoromethanes in the deep equatorial Atlantic. Nature 314, 608–610.

Zangenberg, N., Siedler, G., 1998. Path of North Atlantic Deep Water in the Brazil Basin. J. Geophys. Res. 103, 5419–5428. http://dx.doi.org/10.1029/ 97JC03287.